Title: Binding of heavy metals by oxidised kerogen in (palaeo)weathered black shales

Author: Arkadiusz Derkowski, Leszek Marynowski

Citation style: Derkowski Arkadiusz**,** Marynowski Leszek. (2018). Binding of heavy metals by oxidised kerogen in (palaeo)weathered black shales. "Chemical Geology" (Vol. 493 (2018), s. 441-450), doi 10.1016/j.chemgeo.2018.06.025

Chemical Geology 493 (2018) 441–450

Contents lists available at ScienceDirect

Chemical Geology

journal homepage: www.elsevier.com/locate/chemgeo

Binding of heavy metals by oxidised kerogen in (palaeo)weathered black shales

Arkadiusz Derkowski[a,*], Leszek Marynowski[b]

[a] Institute of Geological Sciences, Polish Academy of Sciences, Senacka 1, 31-002 Kraków, Poland
[b] Faculty of Earth Sciences, University of Silesia, Będzinska 60, 41-200 Sosnowiec, Poland

ARTICLE INFO

Keywords:
Kerogen
Cation exchange capacity
Shale
Weathering
Adsorption
Heavy metals

ABSTRACT

Sub-aerial weathering of black shales drives the gradual leaching of sulphur- and organic-bound heavy metal elements, which are usually abundant in these rocks due to depositional conditions. The formation of oxygen functional groups in kerogen, however, can lead to an opposing mechanism - metal adsorption and binding, similar to a process common in soils. An increase in cation exchange capacity (CEC) measured previously using metal complexes on black shales oxidised under laboratory conditions implies that the same phenomenon may occur in a naturally oxidised black shale. This idea was tested on a unique, well-developed and -preserved Permian palaeoweathering profile containing two neighbouring but diverse black shales from the Devonian/Carboniferous boundary in the Holy Cross Mountains (Poland).

In the studied black shale beds, the oxygen groups formed in kerogen in the partially-weathered zone were found to be responsible for significant changes in adsorption properties measured using hexamminecobalt(III) and Cu(II)-triethylenetetramine cations, which are common probes for CEC. Compared to a pristine part of black shales, the partially weathered zone was depleted of total organic carbon (TOC), sulphur, and sulphur- and organic-bound metals, and highly enriched in Cu, which is generally present in low levels in the nascent shales.

In the partially weathered zone, where TOC content is reduced, apparent CEC values surpass the CECs predicted from the contents and structures of clay minerals, and correlate linearly with the content of oxygen groups developed during weathering. The adsorption properties of carboxyl groups in the oxidised kerogen are suggested as being responsible for the *syn*- or post-weathering enrichment in Cu caused by the remobilisation of older Cu-sulphide ores present in the area. As opposed to natural weathering, aggressive oxidation, e.g. under laboratory conditions produces a high proportion of cross-linked oxygen groups that do not participate in metal cation adsorption. The CEC values of artificially oxidised samples reached a limit corresponding to those of naturally oxidised shales.

Editor: Michael E. Böttcher

1. Introduction

Post-sedimentary oxidation significantly changes the geochemical signatures of organic-rich rocks. With increasing weathering intensity, black shale sections present a gradual depletion of total organic carbon (TOC), sulphur, and most heavy metal elements. Elements bound by organic complexes, e.g. metalloporphyrins (V, Ni, Mo, Re, U), as well as those typically fixed in sulphides (Mo, Cu, Zn, Cd, Pb) are especially prone to leaching at a high rate; thus, results can be observed over a time span of decades (Filby, 1994; Georgiev et al., 2012; Tuttle et al., 2009; Perkins and Mason, 2015). Along with TOC depletion, organic matter (OM) is oxidised via the formation of a C=O bond in kerogen, whereas free and kerogen-bonded hydrocarbons are removed independently (Petsch et al., 2000, 2001; cf. Derkowski and Marynowski, 2016). The remobilised elements are commonly enriched in the regolith or soil zones overlying the weathered shale (e.g., Ling et al., 2015); the mechanism by which redox-sensitive metals are bound by terrigenous and marine sediments has been extensively documented. This binding occurs in oxygenated soils, usually in humic acids, via phenolic and carboxyl functional groups (Senesi and Calderoni, 1988; Benedetti et al., 1996). The same groups are responsible for the elevated cation exchange capacity (CEC) of soils (Parfitt et al., 1995; Kaiser et al., 2008; Rengasamy and Churchman, 1999) and oxidised low-rank coals (Skodras et al., 2014). In extreme cases, it is the oxidised black carbon formed via incomplete combustion of vegetation or fossil fuels that is responsible for high CEC levels in soils (Liang et al., 2006; Cheng et al.,

* Corresponding author.
E-mail address: ndderkow@cyf-kr.edu.pl (A. Derkowski).

https://doi.org/10.1016/j.chemgeo.2018.06.025
Received 4 October 2017; Received in revised form 22 May 2018; Accepted 28 June 2018
Available online 01 July 2018

2006). Oxygen functional groups are formed in both artificially oxidised (under laboratory conditions) and naturally weathered black shale (Landais et al., 1991; Faure et al., 1999; Petsch et al., 2000; Georgiev et al., 2012), and a role has been suggested for them in the transport and accumulation of transition metals (Kawamura and Kaplan, 1987; Marynowski et al., 2017). Weathering of OM-rich rocks, however, does not always result in the depletion of heavy metals. Naturally oxidised low-rank coals are excellent sorbents of heavy metal cations (Kurková et al., 2004; Janoš et al., 2007). Oxidised kerogen is likely to behave similarly to weathered coals or oxidised black carbon, and thus may become a sorbent for metals present in any fluids that migrate through the formation during or after weathering.

Derkowski and Marynowski (2016) found that the same drying regime that produces oxygen functional groups in black shale samples (200 or 250 °C for 18 h under air) also increases the adsorption of hexamminecobalt(III), to levels much higher than those corresponding to the contribution from clay minerals. Upon such an oxidation, the increase in the adsorption of $[Co(NH_3)_6]^{3+}$ cations – broadly used as a probe for CEC in various disciplines of geoscience – correlated closely with the concentration of thermally-generated oxygen groups. Therefore, it was the kerogen surface properties that were found responsible for "excess CEC" (Derkowski and Marynowski, 2016).

The increase in the apparent CEC of a black shale upon mild oxidation under laboratory conditions implies that the same phenomenon occurs in samples oxidised in nature, e.g. during weathering. Oxygen functional groups in weathered kerogen are expected to be responsible for the binding of metal cations in both natural and laboratory (i.e. as an apparent CEC measurement) conditions. The extent of binding is likely to be dependent on the concentration of carboxyl groups. In the present paper we test this hypothesis, using two neighbouring but diverse black shales from the Devonian/Carboniferous boundary which were weathered obliquely to the bedding in the late Permian (Marynowski et al., 2011, 2017). The unique, well-developed and well-preserved palaeoweathering profile in the Kowala quarry (Poland) is detached from the influence of recent soil formation (weathering, pedogenesis), which is known to be a sink for metal cations (Senesi and Calderoni, 1988; Ahmad et al., 2014).

2. Geological setting

An active quarry in Kowala, Holy Cross Mountains (Poland), exposes an open marine sedimentary sequence of Devonian and Carboniferous black shales and carbonates overlain discordantly by Permian conglomerate, several metres thick, and covered by Quaternary deposits (Fig. 1, cf. Marynowski et al., 2011, 2012). Two distinctively different black shale horizons occur in the outcropped sequence: a 10 cm thick Tournaisian (~359–347 Ma) bed and a 100 cm thick late Fammenian (~372–359 Ma) Hangenberg shale. These shales, deposited under diverse (dysoxic vs. anoxic/euxinic, respectively) palaeoenvironmental conditions, are characterised by different organic matter (OM) contents and composition as well as different geochemical redox-sensitive element signatures (Marynowski et al., 2012, 2017). Based on the Rock-Eval pyrolysis data on the unweathered rocks, the bottom layer of the Hangenberg shale contains organic matter of marine origin (type II kerogen), whereas the Tournaisian shale is a mixed type II-III, as also manifested by the occurrence of an assemblage of marine and terrestrial biomarkers (Marynowski et al., 2011, 2012).

The black shales contain a presumably authigenous mixed-layered illite-smectite mineral, rich in illite end-member, as is typical for thermally mature or overmature shales, whereas all OM features and composition (biomarkers, Rock-Eval pyrolysis parameters, vitrinite reflectance) suggest that the sequence is thermally immature to early mature (Marynowski et al., 2011, 2017). Despite conflicting data regarding the degree and time of diagenesis (thermal maturation; cf. Środoń et al., 2009 for a plausible explanation), it is generally agreed that the entire Devonian-Carboniferous section in the Kowala area passed at least a 60 °C isotherm of maximum burial palaeotemperature during the Variscan age (~372 to 330 Ma; Belka, 1990; Narkiewicz et al., 2010).

The weathering profile developed following Variscan folding and late Carboniferous erosion, which discordantly cut the whole sequence at an angle of ~40° (see Fig. 1; Marynowski et al., 2017). Located ~5 m apart, both of these shales are black in the unweathered and 'transitional' or 'partially weathered' zones (see the discussion below for identification of these zones), becoming green-yellow, then reddish, in the 'completely weathered' zone. The colour changes within a few metres as it nears the Permian conglomerates. Primary Cu ores of Variscan age, widespread in the Holy Cross Mts., occur in the Kowala area as sulphide veins. Their likely *syn*-weathering remobilisation is a regionally-recorded event (Rubinowski, 1971).

After the Permian, a Mesozoic marine transgression in the studied part of the Holy Cross Mountains resulted in epicontinental deposits of 2.0 to 3.5 km thick with low geothermal gradients (10–15 °C/km; Belka, 1990; Narkiewicz et al., 2010), ranging from continental clastic to marginal and open marine facies. The maximal palaeotemperatures of Mesozoic burial did not exceed those of Variscan. In the latest Cretaceous and earliest Paleocene, the area of the Holy Cross Mountains underwent tectonic inversion along with other segments of the Mid-Polish Trough. The erosion magnitude was estimated for 2.5–3.5 km of mainly Permo-Mesozoic deposits (Narkiewicz et al., 2010). Based on the geological context as well as on previous studies (Marynowski et al., 2017), the Quaternary position and current exposure of these rocks have no effect on the palaeoweathering sequence. Throughout decades of exploitation, the weathering sequence consisting of the black shale beds overlain by Permian conglomerate has been observed in the Kowala quarry at different spatial positions in respect to the recent weathering front and soil development. Detachment of the paleoweathering profile from post-Paleocene weathering has also been confirmed by palaeomagnetic dating of hematite (of Permian age) occurring in oxidised samples collected several metres below the Permian erosional surface. Also, the Permian age of weathering in the Kowala section is supported by a pattern of chlorite transformations: chlorite occurring in the Permian conglomerate has no signs of vermiculitisation, in contrast to the vermiculitisation observed in chlorite along the black shale weathering transect (Marynowski et al., 2017). The secondary burial and exhumation distinguishes the investigated sequence from the broadly-studied modern weathering of recently exposed black shale beds (e.g. Petsch et al., 2000).

3. Materials and methodology

3.1. Samples

Following the visually distinguishable degrees of weathering, from intact and fresh-looking black shale to red rock at the Permian erosional surface, eight samples were collected from the bottom of the Hangenberg shale and nineteen from the Tournaisian shale (Fig. 1). In both cases, the bottom parts of the shales, 3–4 cm thick, were sampled in order to ensure identical depositional conditions within the investigated bed. The Tournaisian samples used in this study were the same as those collected and studied by Marynowski et al. (2017). All samples were gently crushed to pass a < 0.4 mm sieve, homogenised, and split into representative portions, following the protocol of Środoń et al. (2001).

In addition to using the raw material for various analyses, < 2 μm grain-sized fractions were extracted using chemical purification including carbonate removal, OM oxidation, and Fe-(oxy-)hydroxide removal, followed by centrifugation (Jackson, 1969). The extracted clay fractions were then used for a detailed investigation of clay minerals structure and composition.

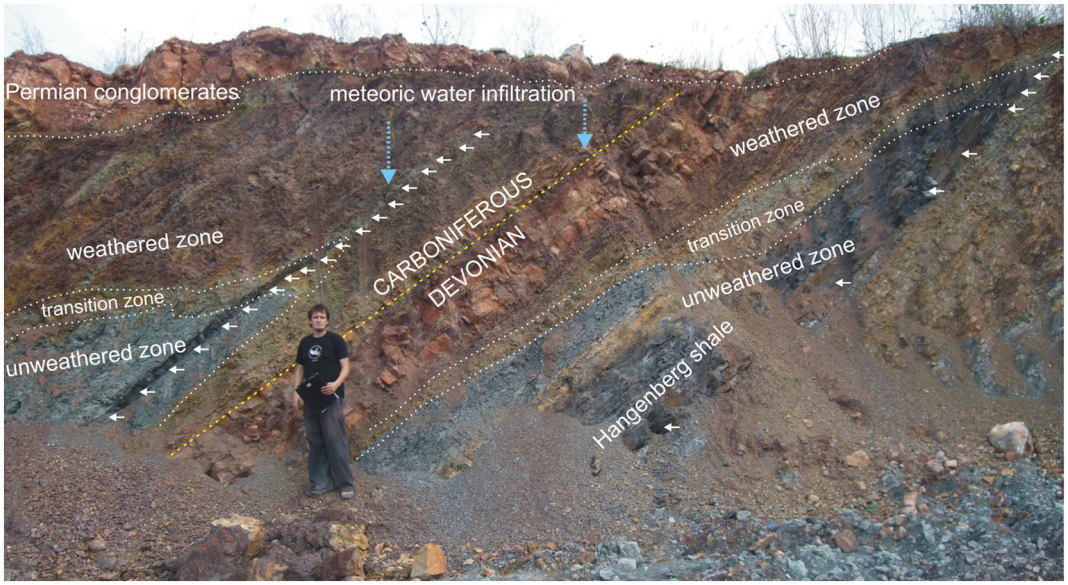

Fig. 1. The studied black shale beds in Kowala Quarry, with arrows denoting the collected samples. See Marynowski et al. (2017) for details of the studied area.

3.2. Methods

Apparent CEC. The definition of CEC requires adsorbed cations to be fully exchangeable. The complex compounds of Co(III) or Cu(II) used to measure CEC have been proven to replace > 95% of exchangeable cations in clays during a single contact (Ciesielski and Sterckeman, 1997; Meier and Kahr, 1999). However, the extent of their adsorption is assumed to be governed predominantly by the cation exchange reaction, which may not be the case in OM-rich rocks. In order to verify the mechanism of hexamminecobalt(III) adsorption, the CEC computed based on the concentration of total exchanged cations (usually Ca, Mg, Na) should equal the CEC determined by the absorbance of supernatant $[Co(NH_3)_6]^{3+}$ solution. If the latter values are greater, it means that either $[Co(NH_3)_6]^{3+}$ has undergone hydrolysis (which, for laboratory-oxidised shales, was rejected by Derkowski and Marynowski, 2016) or that $Co(OH)_2$ precipitation has occurred (Renault et al., 2009). In the case of the studied rocks, however, Ca^{2+} leached from calcite prevents reliable CEC verification (cf. Dohrmann and Kaufhold, 2009). Therefore, a cross-check with Cu(II)-triethylenetetramine solution was performed for the Hangenberg shale samples (Stanjek and Künkel, 2016). Due to the intrinsic problems with verifying the mechanism of Co(III)- and Cu(II)-compound uptake, the measured values are tentatively considered “apparent CEC”.

Hexamminecobalt(III) cations were employed for CEC measurement using a $[Co(NH_3)_6]Cl_3$ solution at pH ~7, following the method of Bardon et al. (1993) and Ciesielski and Sterckeman (1997). A sample split (0.5–1 g) was dried overnight at 60 °C, mixed with 25 ml of the $[Co(NH_3)_6]Cl_3$ stock solution at a known concentration, sonicated for 2 min, shaken for 1 h, and centrifuged for 10 min at ~4000 *g*. The absorbance of the supernatant solutions was analysed with a VIS spectrometer (Helios Gamma, Thermo Scientific) at a wavelength of 470 nm. The supernatant absorbance is linearly correlated with the amount of $[Co(NH_3)_6]^{3+}$ cation remaining in the solution following adsorption by the tested sample. CEC determination with $[Co(NH_3)_6]^{3+}$ was validated using a copper(II)triethylenetetramine (Cu-Trien) solution employing the same principles as above (Stanjek and Künkel, 2016) and wavelengths of 580 and 620 nm.

Three samples, from unweathered and partially weathered zones of the Hangenberg shale, were selected for the additional CEC measurement aimed at testing differing pre-drying conditions under air, following the protocol of Derkowski and Marynowski (2016). Representative portions were dried in under oxidising conditions (air) at 105 °C for 18 h, 200 °C for 20 h, or 200 °C for 25 min.

Chemical analyses. Major oxides and several minor elements were measured using ICP-emission spectrometry at AcmeLabs, Vancouver, Canada. For the analysis, 0.2 g of fine-ground sample was fused with lithium tetraborate; the molten bead was then dissolved in nitric acid, following AcmeLabs in-house protocol. The reliability of analytical results was monitored by means of analyses of international standard reference materials and duplicate analyses of several samples. The precision and accuracy of the results were better than ± 0.05% (mostly ± 0.01%) for the major elements and generally better than ± 1 ppm for the trace elements.

Mineral identification and quantification. For bulk rock phase analysis, the sample splits were spiked with 10% ZnO and milled in a McCrone mill with methanol, following the protocol of Środoń et al. (2001). X-ray diffraction (XRD) analyses were performed using a side-loading holder (to ensure random arrangement of mineral grains), a Thermo ARL X'TRA instrument, and Q-MIN software (by Dr. Marek Szczerba), which uses the mineral intensity factor method in conjunction with a collection of pure standards (Środoń et al., 2001). Structural details of the clay minerals were identified using the XRD patterns collected on oriented specimens of extracted and Ca-exchanged clay fractions, in an air-dried state and following saturation with ethylene glycol (Sakharov et al., 1999).

TOC and OM pyrolysis. Total organic carbon (TOC) was calculated as the difference between total carbon (TC) and total inorganic carbon (TIC). TC, TIC, and total sulphur contents were analysed using an Eltra CS-500 IR-analyser equipped with a TIC module and an infrared cell detector for CO_2 and SO_2 gases evolved from combustion under an oxygen atmosphere. TIC content was derived from carbonates that had reacted with warm 15% hydrochloric acid.

OM pyrolysis was performed using a Rock-Eval 6 apparatus with a standard protocol involving isothermal heating at 300 °C for 4 min followed by ramp heating to 650 °C at a rate of 25 °C/min, enabling determination of S1 and S2 parameters, which correspond to thermovaporised mobile hydrocarbons and those produced by cracking, respectively (Behar et al., 2001). The S3 parameter representing oxygen-bearing OM compounds was quantified by integrating the CO_2 signal within the temperature range corresponding to OM pyrolysis (Derkowski and Marynowski, 2016).

OM extraction, derivatization, and gas chromatography–mass spectrometry (GC–MS). Samples were extracted using a dichloromethane (DCM)/methanol mixture (5:1 v:v) with an accelerated Dionex ASE 350

solvent extractor. Extracts were separated into aliphatic, aromatic, and polar fractions using modified column chromatography (Bastow et al., 2007). The eluents used for collection of the fractions were: *n*-pentane (for aliphatic fractions), *n*-pentane and DCM (7:3; for aromatic fractions), and DCM and methanol (1:1; for polar fractions). All of the solvents used were spectroscopically pure and of super-dehydrated grade. An aliquot of the polar fraction of selected samples was converted to trimethylsilyl derivatives via a reaction with *N*,*O*-bis-(trimethylsilyl)trifluoroacetamide (BSTFA) and pyridine for 3 h at 70 °C.

The GC–MS analyses were carried out with an Agilent Technologies 7890A gas chromatograph and an Agilent 5975C Network mass spectrometer with a Triple-Axis detector (MSD) at the Faculty of Earth Sciences, Sosnowiec. Helium (grade 6.0) was used as a carrier gas at a constant flow of 2.6 ml/min. Gas separation was performed using a J& W HP-5 ms (60 m × 0.32 mm i.d., 0.25 μm film thickness) fused silica capillary column coated with a chemically-bonded phase (5% phenyl, 95% methylsiloxane). The GC oven temperature was programmed from 45 °C (1 min) to 100 °C at 20 °C/min, then to 300 °C (held 80 min) at 3 °C/min, with a solvent delay of 10 min. The GC column outlet was connected directly to the ion source of the MSD. The GC–MS interface temperature was 280 °C, while the ion source and the quadrupole analyser were at 230 and 150 °C, respectively. Mass spectra were recorded at 45–550 Da (0–40 min) and 50–700 Da (> 40 min). The mass spectrometer was operated in the electron impact mode (ionisation energy 70 eV).

An Agilent Technologies MSD ChemStation E.02.01.1177 and Wiley Registry of Mass Spectral Data (9th edition) software were used for data collection and spectra processing. Abundances of *n*-fatty acids were calculated by means of comparison of peak areas of the internal standard (Ethylvanillin) with that of the peak areas of the individual compounds obtained from the GC–MS total ion chromatograms.

4. Results

The mineral composition of the two studied units was similar and typical of this type of rock (Wilson et al., 2016); it is dominated by highly illitic mixed-layered illite-smectite (I-S) mineral, characterised by a stacking order of the R3 type and quartz. Calcite was more abundant in the Hangenberg (24–30%) than the Tournaisian (~12%) shale. There were small percentages of K-feldspar, plagioclase, pyrite, and chlorite. In both shales, pyrite content drops to the values below detection limit within the partially weathered zone, with sulphur content quantitatively following pyrite (Table SI1). As previously observed in the Tournaisian shale (Marynowski et al., 2017), chlorite (~4% of bulk rock) identified in the clay fractions had also undergone vermiculitisation in the weathered zone of the Hangenberg shale. Due to a steady decrease in OM content, from a TOC of ~7% in the Tournaisian bed and ~22% in the Hangenberg shale (Fig. 2) to nearly zero in the partially weathered zone, the relative contents of illite-smectite, feldspars, and quartz increased. Calcite content decreased gradually with weathering to ~7% in the Tournaisian shale, whereas in the Hangenberg bed its content increased up to > 20% in the completely weathered samples, following a significant drop in the transitional zone (Table SI1).

Despite differing Rock-Eval pyrolysis parameters for the nascent OM, both shales followed the same pattern during weathering (Fig. 3). Hydrogen Index (HI; the content of pyrolysable hydrocarbons, S2 over TOC) decreased from ~500 to 10 mg HC/g TOC in the Hangenberg shale and from ~300 to 20 mg HC/g TOC in the Tournaisian bed. The Oxygen Index (OI, a proxy for oxygen groups content in OM, derived from S3/TOC) rose from ~20 mg CO_2/g TOC in both unweathered shales to 350 mg CO_2/g TOC in the Hangenberg and > 170 mg CO_2/g TOC in the Tournaisian shale. S1, representing bulk free hydrocarbon fraction (in mg HC/g rock), decreased linearly with sulphur (Table SI1).

The polar fraction separated from the Hangenberg shale samples was analysed for the occurrence and concentration of non-bonded oxygen compounds. The most abundant oxygen-bearing compounds identified were *n*-fatty acid and *n*-alkane-2-ol homologue series, ranging from C_8 to C_{30} and C_{12} to C_{28}, respectively (Fig. 4). Other compounds, such as *n*-alkane-1-ols or hydroxy-fatty acids, were also identified, in lower abundance. The most abundant compounds were the *n*-fatty acid homologue series, whose total concentration increased from 4.0 to 5.8 μg/g TOC in unweathered shale, reaching a maximum in the transitional zone (10.6 μg/g TOC), and fell to 5.6 μg/g TOC in the highly weathered zone. The changes in *n*-alkane-2-ols content were even more pronounced: their concentration in the unweathered samples ranged from 0.4 to 0.8 μg/g TOC, then increased sharply to 3.2 μg/g TOC before dropping below the detection limit (< 0.01 μg/g TOC) in the weathered sample (Fig. 5).

The concentrations of immobile elements, e.g. Al, Zr, Ti, Rb, Cs, and Th, commonly associated with detrital silicate minerals increase proportionally in the transitional zone (Fig. 2, Table SI1), however, when virtually normalised to the OM-, pyrite-, and carbonate-free mass, the concentrations remained relatively constant along the weathering transect in both shales (cf. Ling et al., 2015; Marynowski et al., 2017). Due to euxinic depositional conditions in a highly restricted basin with elevated productivity (Marynowski et al., 2012), concentrations of certain transition metals were up to several orders of magnitude higher in the Hangenberg shale than in the Tournaisian bed. Among them, the concentrations of Zn, Pb, Mo, Cd, Co, Ni, and As decreased in the Hangenberg shale with weathering following the decrease in sulphur, TOC, and S2 from OM pyrolysis (Fig. 2, Table SI1). Cu reached the highest level of enrichment (more than one order of magnitude) within the partially-weathered zone. In the Tournaisian shale, the patterns of leaching of elements and enrichment upon weathering were described by Marynowski et al. (2017): Cd concentration was below the detection limit; Zn concentration was low, but a minor increase occurred in the completely weathered zone; Mo and As dropped to zero; Ni decreased strongly; Pb varied irregularly, but minor enrichment occurred; and Cu concentration decreased and then became significantly elevated in the partially weathered zone (Table SI1).

Uranium, V, and Hg behaved similarly to Cu; these elements were present in the nascent shale and became enriched in the partially weathered zone; then their concentrations dropped with advanced weathering. However, their degree of depletion and enrichment varies and differ between the two studied shales. In the case of Au, its content in the unweathered shale was either low or below the detection limit, whereas it increased to tens of ppb in the partially weathered zone, and dropped to a few ppb in the weathered zone. In the Hangenberg shale, Au and U enrichments seemed to be shifted towards the weathered zone (Fig. 2, Table SI1).

Apparent CEC measured with hexamminecobalt(III) solution (CEC_{hexCo}) increased from 0.06 and 0.09 meq/g in the unweathered Hangenberg shale to 0.42 meq/g in the transitional zone, dropping below 0.19 meq/g near the Permian surface. A similar, although less extreme trend occurred in the Tournaisian bed: from 0.20 meq/g in nascent shale, CEC increased to 0.34 and dropped to 0.25 meq/g in the weathered zone (Fig. 2). The Cu(II)-Trien adsorption test of the Hangenberg samples resulted in an apparent CEC ($CEC_{CuTrien}$) which, while linearly correlated ($R^2 = 0.98$) with the hexamminecobalt(III) data, reached only 50% of CEC_{hexCo} values in the transitional zone (Fig. 5). In order to test the potential of anionic co-sorption by a $[Co(NH_3)_6]^{3+}$ cation bound to clay or kerogen surfaces, CH_3COONa was added to the $[Co(NH_3)_6]^{3+}$ solution used to measure the CEC of one sample from the partially weathered Hangenberg shale and one reference sample of pure smectite. The concentration of carboxyl groups from the acetate was set to correspond to the concentration of Cl anions. In neither tested sample did the addition of the acetate changed the CEC_{hexCo} beyond the CEC measurement error (0.014 meq/g; Derkowski and Bristow, 2012).

The CEC measurements listed above were performed after drying a sample at 60 °C, i.e. the 'untreated sample' reference. Unweathered and partially weathered samples from the Hangenberg shale did not lose

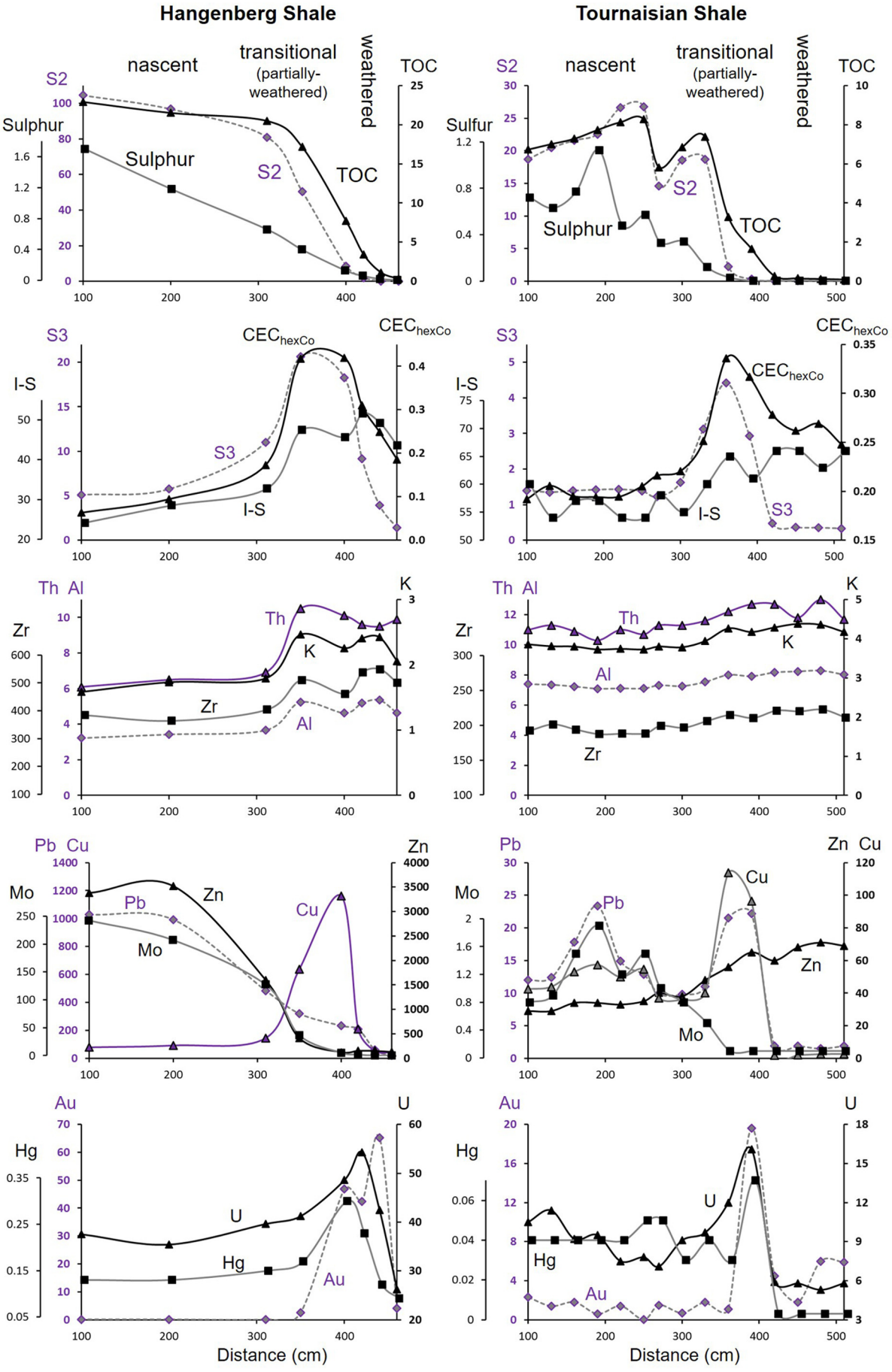

(caption on next page)

Fig. 2. Distribution of major and trace elements, illite-smectite (I-S) mineral, cation exchange capacity measured using hexamminecobalt(III) (CEC_{hexCo}), and Rock-Eval pyrolysis parameters (S2 – pyrolysable hydrocarbons; S3 – oxygen groups), along the weathering profiles of the studied black shale beds. I-S content, total organic carbon (TOC), and concentrations of sulphur, K, and Al are given in wt%, of Au in ppb, and of other trace elements in ppm. S2 is given in mg HC/g rock; S3 in mg CO_2/g rock; CEC_{hexCo} in meq/g.

hydrocarbons or gain oxygen groups when dried overnight at 105 °C. Even short (25 min) drying at 200 °C slightly but consistently increased their OI and decreased their HI values (Fig. 6). Drying for 20 h at 200 °C induced a drop of pyrolysable hydrocarbon content, S2, from 50–100 to 6–8 mg/g TOC, a ~20% relative decrease in TOC, while OI increased to 255–277 mg CO_2/g TOC in all samples. In the samples dried at 105 °C or for 25 min at 200 °C, CEC_{hexCo} values remained similar to those in the untreated portions, whereas long drying at 200 °C caused an instant jump to 0.38 meq/g in the nascent sample and ~0.46 meq/g in the other two partially weathered samples (Fig. 6; Table SI2).

5. Discussion

5.1. Apparent CEC

Because the content and structure of clay minerals determine the bulk rock CEC in an average shale, evaluating the features of these minerals enables calculation of theoretical CEC (cf. Środoń, 2009; Derkowski and Bristow, 2012; Derkowski and Marynowski, 2016). The maximum conservative values contributed by the clay minerals to the bulk rock CEC ($CEC_{Theor(clay)}$) are 0.10 meq/g in the unweathered Hangenberg shale and 0.20 meq/g in the Tournaisian shale. Due to the increase in the relative content of illite-smectite as OM degrades, and due to chlorite vermiculitisation upon weathering, $CEC_{Theor(clay)}$ increases to 0.15 and 0.25 meq/g, respectively, in the weathered zone. These theoretical CEC values closely match the measured CEC in the completely unweathered and completely weathered samples from both beds, but the apparent CEC_{hexCo} measured in the transitional zones exceeds theoretical values significantly (Fig. 5). In the two studied black shales, which are markedly different in origin, age, and composition, an extensive increase in oxygen group content (S3 parameter) in kerogen in the partially weathered zone correlates well with the elevated CEC (Fig. 5). The oxygen groups must therefore be responsible for increased cation adsorption in the rock, similarly to the recent soils (Parfitt et al., 1995; Kaiser et al., 2008). The present study confirms that in naturally-weathered black shale, partially-oxidised OM develops bonds that bind cationic metal complexes, as predicted by Derkowski and Marynowski (2016) based on laboratory oxidised shales.

To track OM changes during weathering, it was assumed at this point that if oxidative weathering caused an increase in the number of COOH and OH functional groups in kerogen, free fatty acids and concentration of alcohols/phenols should be also elevated (cf. Tamamura et al., 2015). Since the Permian weathering, the studied shales were buried at least 2.5 km deep, therefore, the weathered kerogen underwent secondary thermal maturation (Belka, 1990; cf. Narkiewicz et al., 2010), and may have continued to release free organic compounds. Indeed, the concentration of free *n*-fatty acids is almost twice higher in the transitional zone than in the unweathered Hangenberg shale; the pattern of *n*-alkane-2-ols is even more pronounced (Fig. 5). Assuming that these compounds were generated during weathering by precisely the same shale strata (cf. Marynowski et al., 2012), differences in the concentration of *n*-fatty acids (and other oxygen-bearing compounds) would depend on the degree of OM oxidation. Carboxyl and hydroxyl (and other oxygen) functional groups that formed during the first phase of oxidation were subsequently degraded by the advancing weathering front. The elevated concentration of *n*-alkane-2-ols in the transitional zone and less pronounced enrichment of fatty acids suggests that, in the weathered section in Kowala, OM hydroxyl groups may contribute to binding metal complexes along with the carboxyl groups (cf. Kurková et al., 2004; Ahmad et al., 2014).

Various oxygen functional groups may not contribute proportionally to the excess apparent CEC. Their presence in the unweathered samples, as observed in S3 and OI parameter values (Fig. 2, Table SI1), and especially noticeable in the Hangenberg shale, failed to produce an apparent CEC significantly above $CEC_{Theor(clay)}$. It is the oxygen functional groups which were newly formed in the kerogen structure during weathering that bound the CEC probe compounds. The oxygen groups present in the nascent shale can thus occur in an interlinked form or in

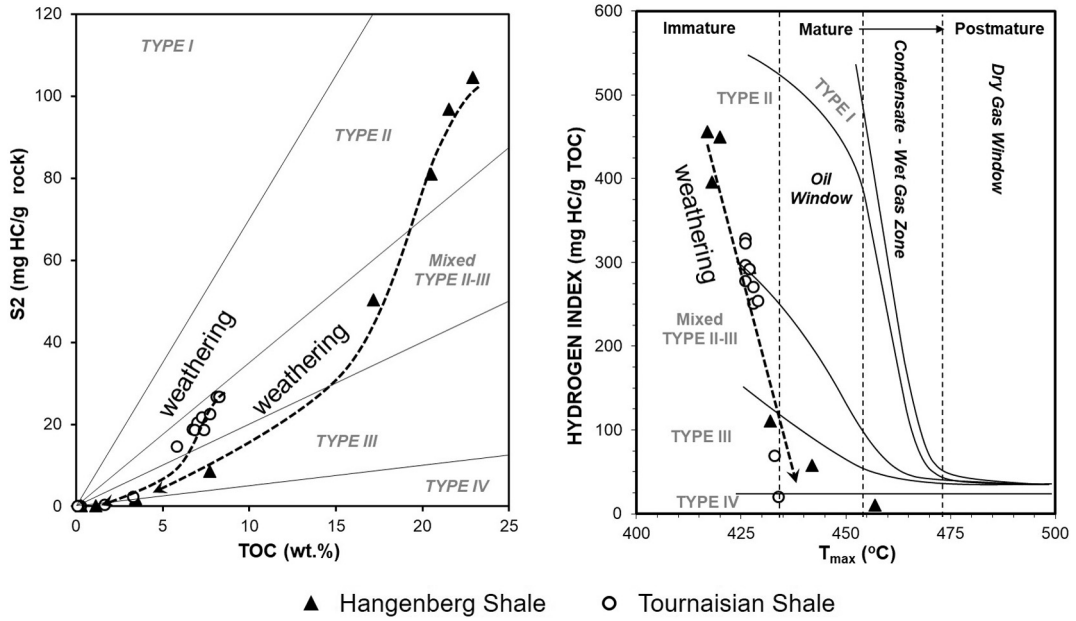

Fig. 3. Rock-Eval pyrolysis data plotted on conventional pseudo-van Krevelen diagrams. Arrows indicate the direction of alteration from the unweathered to the partially weathered zone. Samples from the weathered zone were not analysed due to insufficient TOC content.

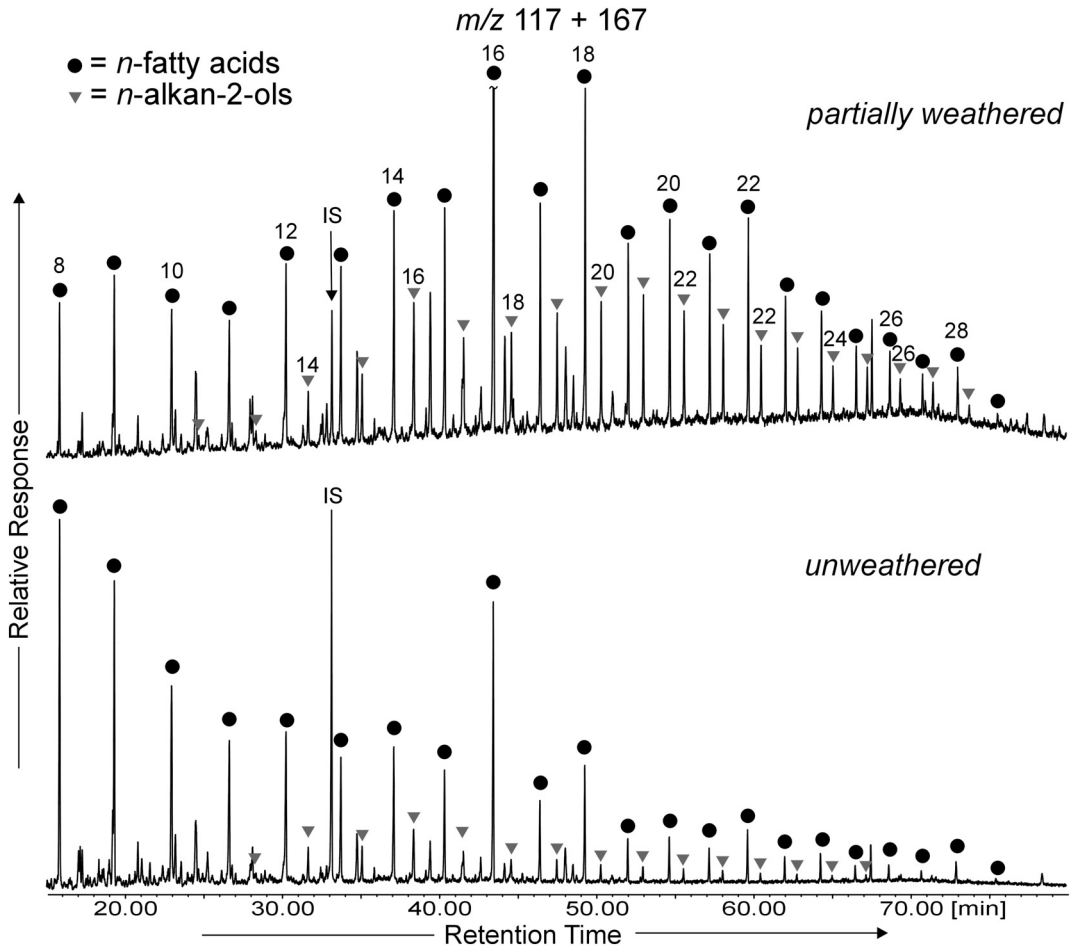

Fig. 4. Summed mass chromatogram for *m/z* 117 + 167, showing the distribution of *n*-fatty acids and *n*-alkano-2-ols in unweathered and partially weathered samples. The same concentration of internal standard (IS) shows differences in compound concentrations. Numbers above peaks indicate C numbers of homologues.

other stable oxygen-containing groups, e.g. furans (Petersen et al., 2008), which would not participate in the adsorption reactions (see a comparison of COOH contents and CEC for different carbonaceous materials in Hanzlık et al., 2004). It is quite possible that OM compounds containing such oxygen groups originating from sedimentary and diagenetic processes undergo decomposition during weathering with a rate proportional to other OM compounds. In contrast to specific recalcitrant OM species that become oxidised (Tamamura et al., 2015), their content likely decreases with TOC during weathering, following the pattern of pyrolysable hydrocarbons (S2) and TOC (cf. Georgiev et al., 2012; Skodras et al., 2014). Therefore, in order to extract the quantity of oxygen groups produced during weathering, the TOC-normalised S3 value of the nascent shale was subtracted from the measured S3 values, proportionally to the sample's TOC. Analogously, the nascent shale's CEC, normalised to the illite-smectite content and an estimated minor contribution from the vermiculitised chlorite, were subtracted from the measured CEC_{hexCo} to estimate the apparent CEC values contributed by OM. The estimated values of excess apparent CEC_{hexCo} and excess S3 that formed during OM weathering, match closely, presenting a common trend in both shales (Fig. 7), thus implying that the newly-formed oxygen groups are responsible for the adsorption of the Co(III) complex cation. In the partially-weathered zones of the two studied shales, the calculated excess CEC divided by TOC (thus corresponding to CEC of OM) reaches 2.2–3.0 meq/gTOC, and even > 5 meq/gTOC in the OM-depleted samples. In the samples featuring high excess CEC and highest contents of newly formed S3, the molar ratio of CEC and pyrolytic CO_2 is close to one (Fig. 7), which strongly supports the tested model of metal cation adsorption by COO^- anion. Indeed, the calculated CEC contribution by oxidised kerogen corresponds to CEC values measured in naturally oxidised lignite and coal (3.3 meq/g; Skodras et al., 2014), soil OM (1.4–10.0 meq/g Kaiser et al., 2008 and references therein), and humic acids present in marine sediments (~3 meq/g; Rashid, 1969). The latter compound was also found as a product of oxidisation in bituminous coals and shales (Kurková et al., 2004; Tamamura et al., 2015), and might have as well be generated by kerogen in the studied black shales.

Natural and artificial OM oxidation produce a common trend of decreased HI with simultaneous OI increase (Fig. 6), matching a pattern observed elsewhere for type II kerogen (Landais et al., 1991). Intense laboratory oxidation, however, does not lead to a drop in TOC content such as is observed in natural samples. Both naturally-weathered and laboratory-oxidised Hangenberg samples reach very similar maximum apparent CEC values (0.42 and 0.47 meq/g, respectively; Fig. 6), but the corresponding content of artificially-produced oxygen groups is more than twice greater than the content produced naturally during weathering (17 vs. 41 $mgCO_2/g$; Fig. 7). The potential of Co(III)-complex binding in the studied black shale features a certain maximum, beyond which the production of more oxygen functional groups does not increase the adsorption capacity. As observed by Derkowski and Marynowski (2016), advanced or aggressive kerogen oxidation forms more cross-linked oxygen groups, such as ethers, that do not participate in Co(III)-complex adsorption.

The excellent match between CEC_{hexCo} and $CEC_{CuTrien}$ values, with both remaining below the $CEC_{Theor(clay)}$ limit, occurs only in the nascent shale (Fig. 5). The difference between the two probe measurements increases linearly with the increased concentration of newly-formed

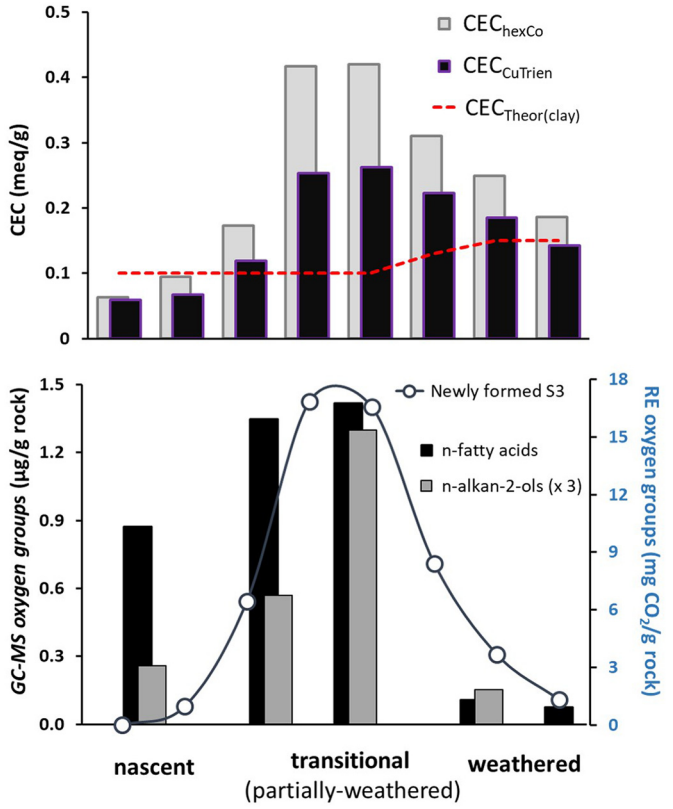

Fig. 5. Distribution of cation exchange capacity (CEC; top) and oxygen groups content measured with GC–MS on a polar fraction extract and with Rock-Eval pyrolysis on a bulk rock (bottom), along the Hangenberg shale's weathering profile. The theoretical estimated contribution of clay minerals to bulk rock CEC is presented along with CEC measured using hexamminecobalt(III) and Cu-Trien cations. Newly-formed S3 represents the oxygen groups measured with Rock-Eval pyrolysis reduced by an estimated S3 contribution from the unweathered portion of OM.

oxygen groups (Fig. 7), which is expected in cases where different mechanisms of binding complex metal cations occur (Benedetti et al., 1996). Whereas complete cation exchangeability and neutralisation of the permanent layer charge is typical of expandable clay minerals (Ciesielski and Sterckeman, 1997; Meier and Kahr, 1999), a variable charge, cation-specific binding, and steric effects are expected for OM (e.g. Ghabbour et al., 2006 cf. Ahmad et al., 2014). As anionic co-sorption by the $[Co(NH_3)_6]^{3+}$ cation was proven negative by a CEC test with CH_3COO^-, other effects specific to oxidised OM may be responsible for this difference, either through reducing the Cu-Trien binding (steric effect, Cu-Trien or Trien protonation; Stanjek and Künkel, 2016) or through virtually increasing hexamminecobalt(III) adsorption (electrochemical reduction and dissociation; $Co(OH)_2$ precipitation; Tomita and Tamai, 1971; Ji et al., 2005; Renault et al., 2009; Hadi et al., 2016). Regardless of the actual reason for the differences in apparent CEC measured with two probes with distinctively different chemical properties, the elevated values occurring in the partially weathered shale represent its potential for binding heavy metal complexes.

5.2. Transition metals enrichment: binding mechanism

Zinc, Pb, Cd, Ni, Co, and Mo constitute the series of redox-sensitive elements whose remarkably distinct concentrations in the pristine shale reflect different geochemical conditions during the deposition of the two formations (Marynowski et al., 2012, 2017). As concentrations of certain transition metals decrease upon weathering along with S and

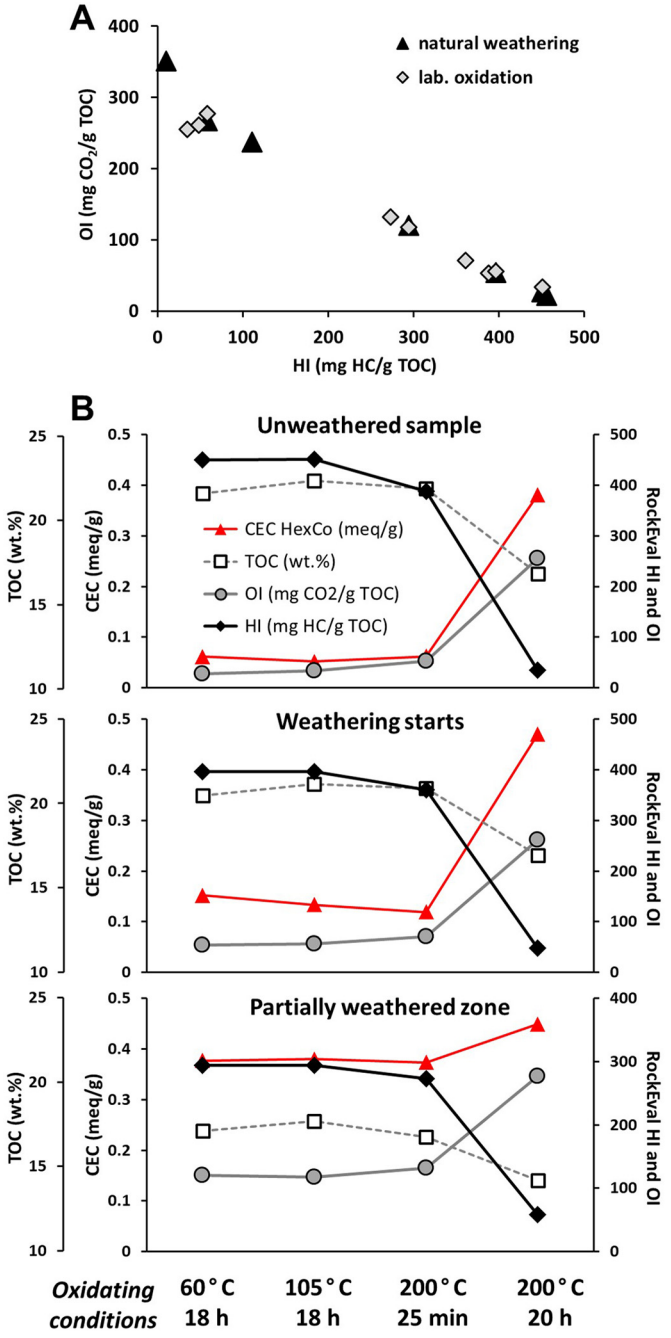

Fig. 6. A) Results of Rock-Eval pyrolysis determined on naturally and artificially weathered (laboratory oxidation) samples from the Hangenberg shale. B) Distribution of pyrolysis parameters presented alongside CEC data as a function of laboratory oxidising conditions for unweathered, slightly weathered, and partially weathered samples.

TOC, in a nascent shale these elements must be bound in sulphides or OM (or both), and are gradually leached out of the shale upon weathering (Table SI1). The decline of sulphur and common S-bound metals' concentrations starts much earlier in the profile than OM oxidation, which occurs abruptly in the zone where S content is already reduced (Fig. 2). This pattern has been observed elsewhere and interpreted as the activity of iron- and sulphide-oxidising bacteria present in the deepest, oxygen-deficient portions of the weathering profile (Petsch et al., 2005). Opposite to sulphides, kerogen requires a high level of oxygen activity and either long exposure or high temperature to trigger oxidation (Petsch et al., 2000; cf. Landais et al., 1991; Faure et al.,

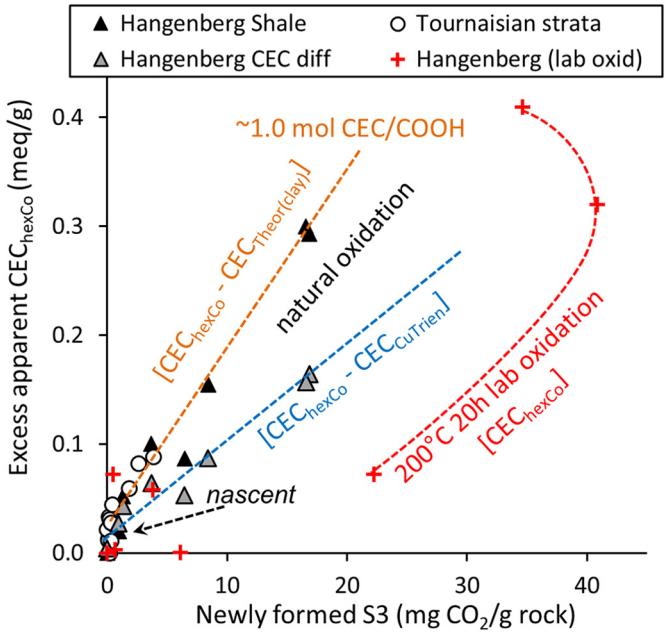

Fig. 7. Excess apparent CEC calculated as CEC_{hexCo} reduced by theoretical CEC contributed by clay minerals ($CEC_{Theor(clay)}$), absolute difference between CEC_{hexCo} and $CEC_{CuTrien}$ (for the Hangenberg shale), and CEC_{hexCo} measured on artificially oxidised Hangenberg samples, all plotted against the content of oxygen groups formed during weathering (cf. Fig. 5).

1999; Rose et al., 1998). As sulphide oxidation in the studied section preceded the formation of oxygen functional groups in kerogen at the progressing weathering front (as measured by the S3 parameter on Fig. 2), the leaching of heavy metals from a particular level was thus already advanced before kerogen oxidation occurred; these two processes may have occurred separately during the period of weathering. Kerogen oxidation most likely took place during the shale's supergene exposure to air, above a groundwater table (cf. Petsch et al., 2000).

Any *in-situ* re-uptake of base metals previously leached from the shale would necessarily involve an assemblage of metals present in the nascent shales (cf. Tuttle et al., 2009). The classical supergene enrichment models (e.g. Ague and Brimhall, 1989) implies that the leaching of metals from the Devonian-Carboniferous suite during intense weathering in the Permian would be followed by their re-concentration in a local basin or a blanket zone. Although some metals (e.g. Pb in the Tournaisian shale) seem to follow the blanket-type enrichment model (Fig. 2), the transition metals composition in the partially weathered zone differs distinctly from that in the nascent shale (e.g. high concentrations of Cu and Au and the lack of significant Zn enrichment). The decrease of OM- and/or S-bound metals concentration followed a pattern commonly observed in recent weathering profiles (Petsch et al., 2000; Tuttle et al., 2009; Perkins and Mason, 2015) and is independent of Cu enrichment. The regional-scale *syn-* or post-weathering remobilisation of the primary Cu-sulphide ores present in the Kowala area (Rubinowski, 1971) seems to be the best candidate for the source of Cu and Au (and – to some extent – Hg and U) enrichment. Nevertheless, any mechanism of enrichment requires a source providing a basin- or section-scale distribution of Cu (Mathur et al., 2012). Because the studied shale beds are only ~5 m apart, any concentration of locally homogenous elements should result in similar availability of metals to both shales. Therefore, a specific mechanism is required to explain the order of magnitude difference in Cu enrichment between the transitional zones of the studied shale beds, given that there is only a twofold difference between their nascent Cu and S concentrations.

Metal sulphide precipitation from oxic fluids when flowing into a reducing environment of OM- and S-rich formations is a commonly observed process. Hydrocarbons serve as H-donors in post-sedimentary mineralisation (Sun and Puttmann, 2000). However, a weathering profile developed independently of metal enrichment offers a different mechanism of immobilisation of heavy metals, using OM adsorption properties. This type of mechanism of heavy metal binding is well known in soils: whereas carboxyl groups are responsible for cation exchange, metal ions reacting with hydroxyls undergo precipitation and hence permanent binding (Benedetti et al., 1996; cf. Ahmad et al., 2014). We suggest that the enrichment of Cu and other redox metals in the studied black shales results primarily from adsorption by oxygen (mostly carboxyl and hydroxyl) groups developed on kerogen surfaces during weathering (cf. Sun and Püttmann, 2001). The proportion of the maximum content of oxygen groups (S3) in the Hangenberg shale to that in the Tournaisian bed (~5:1) roughly corresponds to the proportion of maximum Cu content in these strata (~10:1; Fig. 2). The high reactivity of oxidised OM to heavy metals, reflected by the adsorption of Co(III) and Cu(II) complexes (Fig. 5) serving as CEC probes, supports this hypothesis. The excess CEC_{hexCo} and $CEC_{CuTrien}$ values corresponding to the newly-formed oxygen groups in OM (Fig. 5) work as a proxy for binding metals from metal-rich fluids in the geological environment.

6. Conclusions

The secondary, post-weathering burial under a Mesozoic sequence at least 2.5 km thick and subsequent exhumation caused by Alpine uplift did not alter the Permian weathering profile in two different, Carboniferous and Devonian black shales from the Kowala quarry. The weathering profile characteristics, including the OM surface properties, seem to have remained unchanged since their development (> 250 Ma), closely resembling recently developed weathering profiles of black shales: gradual depletion of sulphur and OM contents, as well as metals bound to these compounds (Zn, Pb, Mo, As). Kerogen in partially-weathered black shale beds was oxidised and the newly-formed oxygen groups were responsible for developing adsorption properties measured using hexamminecobalt(III) and Cu(II)-triethylenetetramine cations, which are common probes for CEC. The elevated values of apparent CEC, exceeding the values predicted from the contents and structures of the clay minerals, are linearly correlated with the oxygen groups developed during shale weathering. Adsorption properties of carboxyl and likely hydroxyl groups in the oxidised kerogen are suggested here as being responsible for the syn- or post-weathering enrichment in Cu and other metals observed in both studied shale beds and caused by remobilisation of older Cu-sulphide ores widespread in the area.

Natural and laboratory oxidation result in identical relationships of removed hydrocarbon groups and newly-formed oxygen groups in kerogen. Aggressive oxidation, however, produces cross-linked oxygen groups that do not participate in the adsorption of metal cations. Due to kinetic differences in the formation of oxygen groups and kerogen oxidative decomposition, artificial high-rate oxidation is not an appropriate analogue for kerogen properties developed during natural weathering.

Acknowledgements

This study was supported by NCN grants: 2011/01/B/ST10/01106 (L.M.) and UMO-2011/03/B/ST10/04602 and the IGSPAS internal grant (A.D.). We thank Prof. Helge Stanjek for discussions and valuable suggestions, and Dr. Michał Rakociński for his help during the fieldwork. The paper was greatly improved following suggestions by Dr. Svetoslav Georgiev and an anonymous reviewer.

Appendix A. Supplementary material: Tables SI1 and SI2

Supplementary data to this article can be found online at https://

doi.org/10.1016/j.chemgeo.2018.06.025.

References

Ague, J.J., Brimhall, G.H., 1989. Geochemical modeling of steady state fluid flow and chemical reaction during supergene enrichment of porphyry copper deposits. Econ. Geol. 84, 506–528.

Ahmad, M., Rajapaksha, A.U., Lim, J.E., Zhang, M., Bolan, N., Mohan, D., Vithanage, M., Lee, S.S., Ok, Y.S., 2014. Biochar as a sorbent for contaminant management in soil and water: a review. Chemosphere 99, 19–33.

Bardon, C., et al., 1993. Recommandations pour la détermination experérimentale de la capacité d'échange de cations des milieux argileux. Rev. Inst. Fr. Pétrol. 38, 621–626.

Bastow, T.P., van Aarssen, B.G.K., Lang, D., 2007. Rapid small-scale separation of saturate, aromatic and polar components in petroleum. Org. Geochem. 38, 1235–1250.

Behar, F., Beaumont, V., Penteado, H.D.B., 2001. Rock-Eval 6 technology: performances and developments. In: Oil & Gas Science and Technology – Revue de l′. 56. Institut Francais du Pétrole, pp. 111–134.

Belka, Z., 1990. Thermal maturation and burial history from conodont colour alteration data, Holy Cross Mountains, Poland. Cour. Forschungsinst. Senck. 118, 241–251.

Benedetti, M.F., Van Riemsdijk, W.H., Koopal, L.K., Kinniburgh, D.G., Gooddy, D.C., Milne, C.J., 1996. Metal ion binding by natural organic matter: from the model to the field. Geochim. Cosmochim. Acta 60, 2503–2513.

Cheng, C.-H., Lehmann, J., Thies, J.E., Burton, S.D., Engelhard, M.H., 2006. Oxidation of black carbon by biotic and abiotic processes. Org. Geochem. 37, 1477–1488.

Ciesielski, H., Sterckeman, T., 1997. A comparison between three methods for the determination of cation exchange capacity and exchangeable cations in soils. Agronomie 17, 9–16.

Derkowski, A., Bristow, T.F., 2012. On the problems of total specific surface area and cation exchange capacity measurements in organics-rich sedimentary rocks. Clay Clay Miner. 60, 348–362.

Derkowski, A., Marynowski, L., 2016. Reactivation of cation exchange properties in black shales. Int. J. Coal Geol. 158, 65–77.

Dohrmann, R., Kaufhold, S., 2009. Three fast new CEC methods for the determination of operationally correct exchangeable calcium cations in calcareous clays. Clay Clay Miner. 57, 251–265.

Faure, P., Landais, P., Griffault, L., 1999. Behavior of organic matter from Callovian shales during low-temperature air oxidation. Fuel 78, 1515–1525.

Filby, R.H., 1994. Origin and nature of trace element species in crude oils, bitumens and kerogens: implications for correlation and other geochemical studies. In: Parnell, J. (Ed.), Geofluids: Origin, Migration and Evolution of Fluids in Sedimentary Basins. Geological Society, London, Special Publications Vol. 78. pp. 203–219.

Georgiev, S., Stein, H.J., Hannah, J.L., Weiss, H.M., Bingen, B., Xu, G., Rein, E., Hatlø, V., Løseth, H., Nali, M., Piasecki, S., 2012. Chemical signals for oxidative weathering predict Re–Os isochroneity in black shales, East Greenland. Chem. Geol. 324–325, 108–121.

Ghabbour, E.A., Shaker, M., Toukhy, A., Abid, I.M., Davies, G., 2006. Thermodynamics of metal cation binding by a solid soil derived humic acid. 2. Binding of Mn(II), Co $(NH_3)_{6aq}^{3+}$ and Hg(II). Chemosphere 64, 826–833.

Hadi, J., Tournassat, C., Lerouge, C., 2016. Pitfalls in using the hexaamminecobalt method for cation exchange capacity measurements on clay minerals and clay-rocks: redox interferences between the cationic dye and the sample. Appl. Clay Sci. 119, 393–400.

Hanzlık, J., Jehlička, J., Šebek, O., Weishauptová, Z., Machovič, V., 2004. Multi-component adsorption of Ag (I), Cd (II) and Cu (II) by natural carbonaceous materials. Water Res. 38, 2178–2184.

Jackson, M.L., 1969. Soil Chemical Analysis – Advanced Course, 2nd Edition. (University of Wisconsin, USA, Published by author).

Janoš, P., Sypecká, J., Mlčkovská, P., Kuráň, P., Pilařová, V., 2007. Removal of metal ions from aqueous solutions by sorption onto untreated low-rank coal (oxihumolite). Sep. Purif. Technol. 53, 322–329.

Ji, X., Chevallier, F.G., Clegg, A.D., Buzzeo, M.C., Compton, R.G., 2005. The electrochemical reduction of aqueous hexamminecobalt (III): studies of adsorption behaviour with fast scan voltammetry. J. Electroanal. Chem. 581, 249–257.

Kaiser, M., Ellerbrock, R.H., Gerke, H.H., 2008. Cation exchange capacity and composition of soluble soil organic matter fractions. Soil Sci. Soc. Am. J. 72, 1278–1285.

Kawamura, K., Kaplan, I.R., 1987. Dicarboxylic acids generated by thermal alteration of kerogen and humic acids. Geochim. Cosmochim. Acta 51, 3201–3207.

Kurková, M., Klika, Z., Kliková, Ch., Havel, J., 2004. Humic acids from oxidized coals I. Elemental composition, titration curves, heavy metals in HA samples, nuclear magnetic resonance spectra of HAs and infrared spectroscopy. Chemosphere 54, 1237–1245.

Landais, P., Michels, R., Kister, J., Dereppe, J.-M., Benkhedda, Z., 1991. Behavior of oxidized type II kerogen during artificial maturation. Energy Fuel 5, 860–866.

Liang, B., Lehmann, J., Solomon, D., Kinyangi, J., Grossman, J., O'Neill, B., Skjemstad, J.O., Thies, J., Luizao, F.J., Petersen, J., Neves, E.G., 2006. Black carbon increases cation exchange capacity in soils. Soil Sci. Soc. Am. J. 70, 1719–1730.

Ling, S., Wu, X., Ren, Y., Sun, C., Liao, X., Li, X., Zhu, B., 2015. Geochemistry of trace and rare earth elements during weathering of black shale profiles in Northeast Chongqing, Southwestern China: their mobilization, redistribution, and fractionation. Chem. Erde-Geochem. 75, 403–417.

Marynowski, L., Kurkiewicz, S., Rakociński, M., Simoneit, B.R.T., 2011. Effects of weathering on organic matter: I. Changes in molecular composition of extractable organic compounds caused by paleoweathering of a Lower Carboniferous (Tournaisian) marine black shale. Chem. Geol. 285, 144–156.

Marynowski, L., Zatoń, M., Rakociński, M., Filipiak, P., Kurkiewicz, S., Pearce, T.J., 2012. Deciphering the upper Famennian Hangenberg Black Shale depositional environments based on multi-proxy record. Palaeogeogr. Palaeoclimatol. Palaeoecol. 346-347, 66–86.

Marynowski, L., Pisarzowska, A., Derkowski, A., Rakociński, M., Szaniawski, R., Środoń, J., Cohen, A.S., 2017. Influence of palaeoweathering on trace metal concentrations and environmental proxies in black shales. Palaeogeogr. Palaeoclimatol. Palaeoecol. 472, 177–191.

Mathur, R., Jin, L., Prush, V., Paul, J., Ebersole, C., Fornadel, A., Williams, J.Z., Brantley, S., 2012. Cu isotopes and concentrations during weathering of black shale of the Marcellus Formation, Huntingdon County, Pennsylvania (USA). Chem. Geol. 304, 175–184.

Meier, L., Kahr, G., 1999. Determination of the cation exchange capacity (CEC) of clay minerals using the complexes of copper(II) ion with triethylenetetramine and tetraethylenepentamine. Clay Clay Miner. 47, 386–388.

Narkiewicz, M., Resak, M., Littke, R., Marynowski, L., 2010. New constraints on the Middle Palaeozoic to Cenozoic burial and thermal history of the Holy Cross Mts. (Central Poland): results of numerical modeling. Geol. Acta 8, 189–205.

Parfitt, R.L., Gilltrap, D.J., Whitton, J.S., 1995. Contribution of organic matter and clay minerals to the cation exchange capacity of soils. Commun. Soil Sci. Plant Anal. 26, 1343–1355.

Perkins, R.B., Mason, Ch.E., 2015. The relative mobility of trace elements from short-term weathering of a black shale. Appl. Geochem. 56, 67–79.

Petersen, H.I., Rosenberg, P., Nytoft, H.P., 2008. Oxygen groups in coals and alginite-rich kerogen revisited. Int. J. Coal Geol. 74, 93–113.

Petsch, S.T., Berner, R.A., Eglinton, T.I., 2000. A field study of the chemical weathering of ancient sedimentary organic matter. Org. Geochem. 31, 475–487.

Petsch, S.T., Smernik, R.J., Eglinton, T.I., Oades, J.M., 2001. A solid state ^{13}C-NMR study of kerogen degradation during black shale weathering. Geochim. Cosmochim. Acta 65, 1867–1882.

Petsch, S.T., Edwards, K.J., Eglinton, T.I., 2005. Microbial transformations of organic matter in black shales and implications for global biogeochemical cycles. Palaeogeogr. Palaeoclimatol. Palaeoecol. 219, 157–170.

Rashid, M.A., 1969. Contribution of humic substances to the cation exchange capacity of different marine sediments. Marit. Sed. 5, 44–50.

Renault, P., Cazevieille, P., Verdier, J., Lahlah, J., Clara, C., Favre, F., 2009. Variations in the cation exchange capacity of a ferralsol supplied with vinasse, under changing aeration conditions: comparison between CEC measuring methods. Geoderma 154, 101–110.

Rengasamy, P., Churchman, G.J., 1999. Cation exchange capacity, exchange cations and sodicity. In: Peverill, K.I., Sparrow, L.A., Reuter, D.J. (Eds.), Soil Analysis, an Interpretation Manual. CSIRO Publishing, Australia, pp. 147–157.

Rose, H.R., Smith, D.R., Vassallo, A.M., 1998. Study of the oxidation of oil shale and kerogen by Fourier transform infrared emission spectroscopy. Energy Fuel 12, 682–688.

Rubinowski, Z., 1971. The non-ferrous metals of the Świętokrzyskie Mountains and their metallogenic position (in Polish with English summary). Biul. Inst. Geol. 247, 1–139.

Sakharov, B.A., Lindgreen, H., Salyn, A.L., Drits, V.A., 1999. Determination of illite-smectite structures using multispecimen X-ray diffraction profile fitting. Clay Clay Miner. 47, 555–566.

Senesi, N., Calderoni, G., 1988. Structural and chemical characterization of copper, iron and manganese complexes formed by paleosol humic acids. Org. Geochem. 13, 1145–1152.

Skodras, G., Kokorotsikos, P., Serafidou, M., 2014. Cation exchange capability and reactivity of low-rank coal and chars. Open Chem. 12, 33–43.

Środoń, J., 2009. Quantification of illite and smectite and their layer charges in sandstones and shales from shallow burial depth. Clay Miner. 44, 421–434.

Środoń, J., Drits, V.A., McCarty, D.K., Hsieh, J.C.C., Eberl, D.D., 2001. Quantitative XRD analysis of clay-rich rocks from random preparations. Clay Clay Miner. 49, 514–528.

Środoń, J., Clauer, N., Huff, W., Dudek, T., Banaś, M., 2009. K-Ar dating of the Lower Palaeozoic K-bentonites from the Baltic Basin and the Baltic Shield: implications for the role of temperature and time in the illitization of smectite. Clay Miner. 44, 361–387.

Stanjek, H., Künkel, D., 2016. CEC determination with Cutriethylenetetramine: recommendations for improving reproducibility and accuracy. Clay Miner. 51, 1–17.

Sun, Y.-Z., Puttmann, W., 2000. The role of organic matter during copper enrichment in Kupferschiefer from the Sangerhausen basin, Germany. Org. Geochem. 31, 1143–1161.

Sun, Y.-Z., Püttmann, W., 2001. Oxidation of organic matter in the transition zone of the Zechstein Kupferschiefer from the Sangerhausen Basin, Germany. Energy Fuel 15, 817–829.

Tamamura, S., Ueno, A., Aramaki, N., Matsumoto, H., Uchida, K., Igarashi, T., Kaneko, K., 2015. Effects of oxidative weathering on the composition of organic matter in coal and sedimentary rock. Org. Geochem. 81, 8–19.

Tomita, A., Tamai, Y., 1971. Effect of surface groups of carbon on the adsorption and catalytic base hydrolysis of a hexaamminecobalt(III) ion. J. Phys. Chem. 76, 649–654.

Tuttle, M.L., Breit, G.N., Goldhaber, M.B., 2009. Weathering of the New Albany Shale, Kentucky: II. Redistribution of minor and trace elements. Appl. Geochem. 24, 1565–1578.

Wilson, M.J., Shaldybin, M.V., Wilson, L., 2016. Clay mineralogy and unconventional hydrocarbon shale reservoirs in the USA. I. Occurrence and interpretation of mixed-layer R3 ordered illite/smectite. Earth Sci. Rev. 158, 31–50.